Structural and Radio Frequency Co-Design and Optimization of Large Deployable Reflectarrays for Space Missions

Andrea Guarriello, Renaud Loison, Daniele Bresciani, Hervé Legay, George Goussetis

Structural and Radio-Frequency Co-design and Optimization of Large Deployable Reflectarrays for Space Missions

Andrea Guarriello, Renaud Loison, Daniele Bresciani, Hervé Legay, George Goussetis, *Senior Member, IEEE*

***Abstract*—The structural and Radio-Frequency (RF) design and optimization of a large deployable faceted reflectarray (RA) generating double polarization contour beam are presented in this work. The issue addressed is the thermoelastic stability of large RAs and the impact of the thermoelastic deformation (TED) under transverse thermal gradient on the RA performances. Finite elements TED analysis are conducted on a deployable RA with self-standing structures, demonstrating the detrimental effects of the in-orbit TED impact on the RA performances, estimated to be above 3 dB losses. To this extent, a novel structural solution is proposed, based on the employ of reliable mechanical support capable to mitigate the TED. The mechanical design reorientation is contingent on the RF design reformulation. The proposed novel mechanical and RF co-design concept and methodology allows the conception of a low profile, thermo-structurally stable RA with compliant radiation patterns and high cross-polarization discrimination in the worst-case thermal load. This methodology is based on a direct optimization of nine panels faceted RA composed of advanced high-order Phoenix cells directly optimized to fulfill the contoured beam requirements and by respecting the local periodicity requirements of the layout.**

***Index Terms*—Large Deployable Reflectarray, Thermoelastic Deformation, Contoured Beam, Satellite Antenna, Optimization, Phoenix Cells.**

I. Introduction

LARGE space structures are increasingly taking place in recent past and present space missions. Missions require more and more challenging communication links. Large antenna reflectors for broadcast link and synthetic aperture radar for altimeter payloads can be cited as typical examples of large spacecraft subsystems. The dimensions of these structures do not allow them to be allocated in the limited volume of a launcher fairing. Typically, reflectors larger than 4 m cannot be stowed in the launcher fairing. Therefore, it is necessary to conceive such antennas as foldable, stow them in the launcher fairing during the launch phase, and deploy them while in orbit.

The alternatives to very large aperture reflectors are deployable reflectarray (RA) antennas [1], [2] and deployable mesh reflectors [3]. Mesh reflectors require a large hand assembly and represent a costly solution [4]. Moreover, to generate contour beam radiation patterns, mesh reflectors do not allow high levels of surface shaping. For this reason, they need a feeding cluster that increases the cost and the mass of the antenna system. Current advances show the complexity of a mesh reflector shaping [5]. Deployable RA antennas allow to design very large physical aperture single-feed reflectors, typically up to $6-7$m [1]. They can rely on existing technology, such as deployable flat panels as for solar generators [1] or deployable membranes as for solar sails [2]. Deployable RA antennas may open new frontiers in the design of large space antennas since they are lightweight, flat, cost-effective and they do not need a complex feeding network to produce advanced contour beam patterns [6].

Nevertheless, RAs suffer from some limitations, such as the lack of high thermoelastic stability of state-of-the-art low radio-frequency (RF) losses composite panels. In the case of large space RAs, thermoelastic stability is a challenging issue, since large structures are more sensitive to thermal gradients. The reflecting surface must remain as stable as possible in terms of deformations in order to preserve the nominal RF performance. The thermoelastic stability of RAs issue has been addressed in previous works for small panels (operating at frequencies above X-band) with multilayer structures [7], [8], [9] and with single-layer structures [10], [11], [12], [13]. In [7], [8], the RA thermoelastic stability is ensured by bulky carbon fiber reinforced plastic (CFRP) composite panels mechanical support on which the multilayer electrical panel is directly bonded. The reduced panel sizes (1036×980 mm) and the high stiffening panel/RF panel thickness and stiffness ratio (30mm over 6 mm), united to the similar coefficient of thermal expansion (CTE) materials employed, allow the direct bonding without causing, or considerably limiting, the bi-material effect [14], which causes thermoelastic deformations (TED) even at room temperature for materials with different CTE directly bonded together. However, this solution cannot be envisaged for larger panels since it would dramatically increase the mass and the volume and a membrane/flexion coupling may occur [15]. In [9] the considered mechanical support consists of three layers of Quartz fiber, a 30 mm Quartz honeycomb core, and another three layers of Quartz

This work was supported by the European Commission through the H2020 Project REVOLVE under Grant MSCA-ITN2016-722840. The authors would like to thank Jean-Francois David, Eric Labiole, Renaud Chiniard and Christophe Fabries from Thales Alenia Space for supplying fundamental data and for the fruitful discussions.

Andrea Guarriello (corresponding author) and Renaud Loison are with the Institut d'Electronique et des Technologies du numéRique (IETR), National Institute of Applied Sciences (INSA),35708 Rennes, France (e-mail: andrea.guarriello@insa-rennes.fr; renaud.loison@insa-rennes.fr).

Daniele Bresciani and Hervé Legay are with are with Thales Alenia Space, 31037 Toulouse, France (e-mail: daniele.bresciani@thalesaleniaspace.com; herve.legay@thalesaleniaspace.com).

George Goussetis is with the Institute of Sensors Signals and Systems, Heriot-Watt University, Edinburgh EH14 4AS, U.K. (e-mail: g.goussetis@hw.ac.uk).

This article has been accepted for publication in IEEE Transactions on Antennas and Propagation. This is the author's version which has not been fully edited and content may change prior to final publication. Citation information: DOI 10.1109/TAP.2023.3247940

fiber where the RF panel is directly bonded. Although the improved stiffness of the whole assembly, TED were severe because of the quartz CTE, which is quite higher compared to CFRP. Moreover, important residual TED after thermal cycling caused non-negligible distortions in the measured radiation patterns. The residual TED observed even at room temperature may suggest that the asymmetric composite stack, in which the mechanical support is directly bonded on the RF panel with a thickness/stiffness ratio lower than in [7], [8], incurs into bi-material effect. To avoid bi-material and membrane/flexion coupling effects, symmetrical stacks with a redundant RF panel on the stiffening panel back-side have been proposed [10], [11], [12], [13], where a low CTE CFRP mechanical support is sandwiched between two identical RF panels. For lower frequency and large physical aperture applications, this solution would dramatically increase the volume and the mass of the deployable RA. Another recent work [16] presents a large-aperture deployable RA in S-band (5×1 m) design and scaled realization with self-standing structures. The TED analysis shows important deformations under a transverse thermal gradient of $10°C$ (considered as a worst case) of roughly 11 mm (0.13 times the RF wavelength), which would certainly degrade the RF performances. Unfortunately, the TED impact on RA radiation patterns is not surveyed in this work.

The scope of this paper is to propose a new suitable and reliable structural solution for the design of large deployable RAs. The proposed solution aims to mitigate the TED issue, surveyed through a TED structural analysis. TED effects on the RA RF performances are taken into account and the RF synthesis is adapted to the novel mechanical design. To this extent, this original approach based on coupled structural/RF design is applied to conceive a large single-layer deployable RA. The proposed antenna works in double circular polarization in S-band for GEO broadcast application.

The paper is structured as follows. Section II presents the use-case mission requirements, the antenna geometry, the finite elements model employed in structural analysis and the considered thermal load cases. In section III the RF/thermo-mechanical analysis and design of a conventional single-layer deployable RA with self-standing structures is presented. Section IV deals with the mechanical solution proposed in this paper to mitigate the TED and the impact on the RF performances and design. The novel RA with a mechanical support RF/thermo-mechanical design and optimization is presented in section V, with particular attention to the double circular polarization requirement in the RF design.

II. Mission, antenna system and considered thermal load

A. Antenna mission

The use-case coverage region is defined by a set of ground-station distribution covering the Continental United States geographical region (CONUS). The targeted performances are summarized in the table I below. They are defined by the far-field of a 6 m metallic reference reflector previously optimized, illuminated by a circularly polarized feed.

TABLE I: Target Mission

Orbit/mission	Geostationary/broadcast satcom
Coverage type	Shaped CONUS beam
Polarization	Double circular *RHCP-LHCP*
Bandwidth	0.85% S-band $2320 - 2340$ MHz
Central frequency	$f_0 = 2330$ MHz
G_{min} on conus	25 dB

B. Antenna architecture

The RA geometry considered is depicted in Figure 1. In Figure 1b the panels gap has been exaggerated in order to better highlight the 9 panels separation. In practice, the panels edges are separated by a very small gap, of the order of 5 mm. The faceted RA imitates the conformal shape of the conventional 6 m reference reflector in order to mitigate the differential spatial phase delay that should be supplied if the RA was flat. This choice is adopted for frequency bandwidth purposes [17]. An offset feed configuration illuminates the RA. The RA geometrical features are summarized in table II. The RA is deployable thanks to a system of high-precision hinges and the deployment scheme presented in [18].

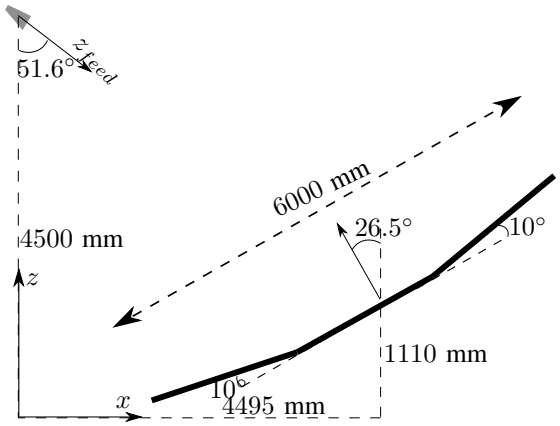

(a) Side view of the antenna geometry.

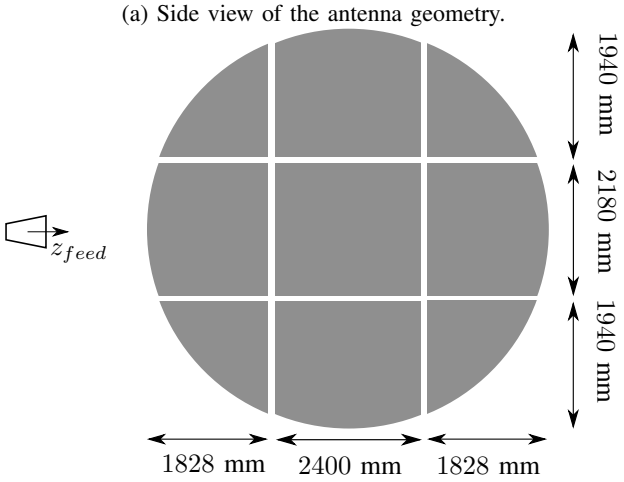

(b) Upper view of the antenna geometry.

Fig. 1: Schematic representation of the deployed RA antenna geometry.

This article has been accepted for publication in IEEE Transactions on Antennas and Propagation. This is the author's version which has not been fully edited and content may change prior to final publication. Citation information: DOI 10.1109/TAP.2023.3247940

TABLE II: RA features

RA geometry	circular
Number of flat panels	9
Overall physical aperture	$D_x = D_y = 6\,m$
Focal distance	4500 mm
Offset distance	4350 mm
Clearance	174.5 mm

C. RA in deployed configuration finite elements model for TED analysis

The finite elements model (FEM) is constructed and post-processed in commercial software MSC Patran and analyzed in MSC Nastran [19], which are the industry's standard tools for structural FEM analysis. The panels are modeled through two main elements: shell elements, modeling the panels skins, and 3D solid elements, modeling the panels' core. Each rectangular panel mesh is composed of 20×20 surface nodes and 5 nodes along the transverse direction. Triangular panels (corner panels) are discretized with 20 nodes on each side and 5 nodes along the transverse direction. Each panel node is attached to the specific panel reference frame, defined as in the RA electrical model, used in the RF computations. Figure 2 shows the FEM built in MSC Patran.

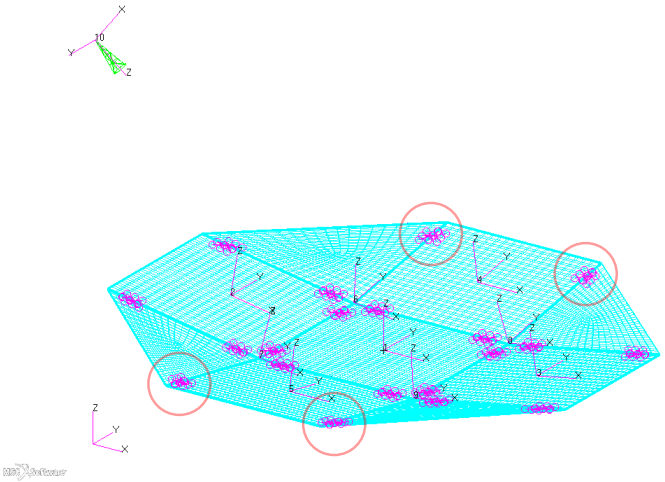

Fig. 2: Complete FEM of the nine panel RA in the deployed configuration. Encircled in red the locking devices.

By looking at Figure 2, we can notice the interfaces connecting the panels in violet. These interfaces represent the hinges and locking devices (the latter encircled in red). The hinges design was not included in this work, but pre-existing enhanced hinges are considered, coming from the heritage on deployable solar generators [1]. The locking mechanism is based on the concept presented in [18] based on permanent magnets. Indeed, the lateral panels cannot be connected through the hinges to respect the deploying mechanisms. Therefore, it is necessary to lock together these panels through a clever concept, as proposed in [18]. The hinges and the locking devices are modeled as rigid elements (Nastran RBE2, option LAGRANGE for the TED analysis) and elastic interfaces (Nastran CELAS1). The rigid elements connect 5 slave nodes belonging to each panel's rear skin to a master node that represents the interface node between the two adjacent panels' faces. The master nodes of the two interfaced panels are rigidly connected to two coincident (same position in the same reference frame-hinge local frame) and distinct nodes. Therefore, these two coincident nodes are connected through a flexible interface, representing the hinges' equivalent elasticity (translational and rotational). The locking devices are modeled through the same methodology with adapted elastic constants. For the thermo-elastic study, the hinges and the locking devices are considered as composed of a titanium alloy, presenting a CTE close to the ones of the composite panels (CTE$= 9 \times 10^{-6} °C^{-1}$), aiming to mitigate pre-tensioning stresses ate the panel/hinges interfaces.

Concerning boundary conditions, the model is constrained on the feed proximity panel. More specifically, the panel in the proximity of the feed is constrained by clamping the 6 d.o.f. on 9 rear surface nodes, covering a surface of roughly 200 mm $\times$ 200 mm. This modeling aims to reproduce the reflector arm holding the RA when deployed through the holding and release mechanisms. The mechanical FEM takes into account the deployment scheme presented [18].

D. Thermal load case modeling

The thermal load cases considered in this work are issued from an in-orbit thermal study and supplied as a conservative worst-case which takes into account the thermal transients cycles along an entire geostationary orbit and a passive thermal control system. It is modeled as a linear transversal thermal gradient of 20° established between the front and the rear skins of the panels (along the panels thickness). In this study, we consider that a transversal thermal gradient is uniformly distributed on the RA panels surfaces by neglecting the shadowing of other spacecraft components that can take place during the eclipse entering or exit, or during other orbital phases. The considered thermal load cases are listed in table III.

TABLE III: List of considered thermal load cases

Thermal load case	**Transversal thermal gradient**
eclipse exit (EX)	$T^{front} = 20°\text{C}$, $T^{rear} = 40°\text{C}$
eclipse entering (EN)	$T^{front} = 40°\text{C}$, $T^{rear} = 20°\text{C}$
cold case EX	$T^{front} = -100°\text{C}$, $T^{rear} = -80°\text{C}$
hot case EX	$T^{front} = 100°\text{C}$, $T^{rear} = 120°\text{C}$
cold case EN	$T^{front} = -80°\text{C}$, $T^{rear} = -100°\text{C}$
hot case EN	$T^{front} = 120°\text{C}$, $T^{rear} = 100°\text{C}$

III. Design and Analysis of a Classical RA with Self-Standing Structure

In this section, the mechanical model construction and analysis and the RF analysis and design of a large deployable RA composed of panels with self-standing structure [1] are addressed. The objective of this classic design is to assess the impact of in-orbit thermoelastic deformation under a transverse thermal gradient on the RF performances in terms of gain losses on the ground stations.

This article has been accepted for publication in IEEE Transactions on Antennas and Propagation. This is the author's version which has not been fully edited and content may change prior to final publication. Citation information: DOI 10.1109/TAP.2023.3247940

A. Mechanical features

The materials and the related industrial processes of the RA with self-standing structure have been deeply surveyed in previous studies [1], [9], [20]. The composite panels layup is shown in Figure Figure 3. It consists of a sandwich panel composed of a low RF losses honeycomb based on quartz fiber material. The composite panels are composed of a multi-layer structure characterized by symmetry, necessary to ensure the panels' mechanical properties. Composite structures macro-mechanics [21] demonstrates that symmetric structures enable to decouple the in-plane to the out-of-plane behavior in order to fully exploit the composite structure mechanical properties without incurring in undesired stress-deformation of different nature coupling, through the stiffness matrices. In general, for a composite panel, the constitutive relations between forces/moments and translation/rotation deformations are written.

$$\begin{Bmatrix} \bar{N} \\ \bar{M} \end{Bmatrix} = \begin{bmatrix} \bar{\bar{A}} & \bar{\bar{B}} \\ \bar{\bar{B}} & \bar{\bar{D}} \end{bmatrix} \begin{Bmatrix} \bar{\varepsilon_0} \\ \bar{\zeta} \end{Bmatrix} \tag{1}$$

where $\bar{N}$ is the in-plane or membrane solicitation vector, $\bar{M}$ is the flexo-torsional solicitation vector, $\bar{\varepsilon_0}$ and $\bar{\zeta}$ respectively the in-plane and out of plane deformations. For a symmetric stack, the stiffness coupling matrices $\bar{\bar{B}}$ are null. Some other terms of the matrices $\bar{\bar{A}}$ and $\bar{\bar{D}}$, linking in-plane solicitation with out-of-plane deformation (and vice-versa), are null as well for symmetric and balanced panels, as in our case. To be more precise, the ground plane layer and the cells metallic grid are not completely identical. Given the very limited impact of the copper thin layers on the composite mechanical properties, we can assume the stack is symmetric. In general, for the studied case, a symmetric composite stack allows to avoid that in-plane thermal gradients generate out-of-plane deformations and, vice-versa, transversal thermal only generates out-of-plane deformations.

The Astroquartz fabrics [22] are used as low RF losses stiffening skins, while the copper ground-plane and the copper cells are directly etched on the sandwich skins. A thin layer of protecting Kapton is used to avoid direct metal exposure to the space environment. The panel thickness is roughly 30 mm, which corresponds to $\lambda_0/4$, where λ_0 is the free-space wavelength at the central operational frequency $f_0 = 2330$ MHz.

B. Phoenix cells lookup table

The RA cells lattice size is fixed to $p = 43$ mm, corresponding to $\lambda_0/3$. The cell topology is shown in Figure 3. As array element geometric pattern, the square loop/slot periodic cycle on the bottom of Figure 4 is considered, which represents first and second-order inductive Phoenix cells [23], [24]. This cycle allows to avoid sharp geometrical transitions for adjacent cells showing similar reflection properties. Figure 4 shows the behavior of the cells as a function of the auxiliary periodic variable ξ defined as a linear periodic parametrization of the square patch or slot sizes as represented in the inset of Figure 4. The cells scattering behavior is characterized by considering each cells as part of a periodic environment,

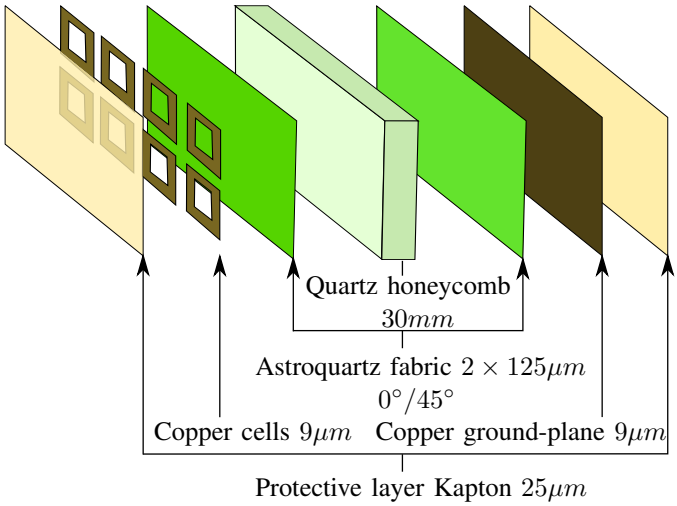

Fig. 3: RA composite panels layup.

which implies that the RA layout must be quasi-periodic. In [25], a systematic study of the global effects of having a layout composed of sharp geometrical transition on the RA performance predictability shows that the local periodicity hypothesis is a constraint in the RA design. The cell samples composing the lookup table are fully characterized in reflection by exploiting an industrial in-house spectral domain Method of Moments software [26], [27]. In Figure 4, the reflection phase is calculated under oblique plane wave incidence $\theta^{inc} = 25°$, $\phi^{inc} = -180°$ and displayed as a function of the parameter ξ. The lookup table is computed for all the incidences relative to the RA geometry evaluated in the RA analysis. The variation of the phase curves shows that an almost complete $360°$ phase cycle is achieved. The maximum and minimum values of d_1 and d_2 are bounded in order to avoid geometries that would not be realizable.

In order to preserve the incident field polarization, the reflecting cells should not have a depolarizing effect, i.e., the phase difference between the main reflection matrices coefficients $\angle\Gamma_{TETE} - \angle\Gamma_{TMTM}$ should be as small as possible. Figure 4b shows this phase difference for each geometry. We can notice that by increasing the local incidence angle, the cells show a marked difference between $\angle\Gamma_{TETE}$ and $\angle\Gamma_{TMTM}$. The region of the RA that mostly reflect the incident energy is the central panel, which sees the incident field with an incidence of about $\theta^{inc} = 25°$. The cells of the lookup table show a light depolarizing effect ($(\Gamma_{TETE} - \Gamma_{TMTM})_{max} = \pm 5°$). In the first instance, we estimate that it is acceptable to not alter the reflected field polarization purity. This kind of cell is used also for alternative applications, such as the reduction of specular reflection [28].

C. RA synthesis methodology and results

The RA design is performed by considering the RA surface as a $2D$ distribution of the ξ periodic parameter.

The process is performed in two steps. The first step is based on a classical phase-only (PO) synthesis. For each cell, the ideal phase of the two aperture field components E_x^{refl}

This article has been accepted for publication in IEEE Transactions on Antennas and Propagation. This is the author's version which has not been fully edited and content may change prior to final publication. Citation information: DOI 10.1109/TAP.2023.3247940

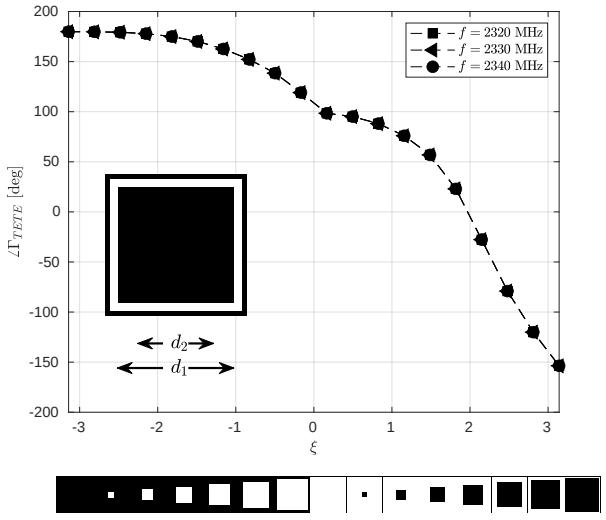

(a) Lookup table 1 cells reflection phase with respect to different frequencies at incidence $\theta^{inc} = 25°$ and $\phi^{inc} = -180°$.

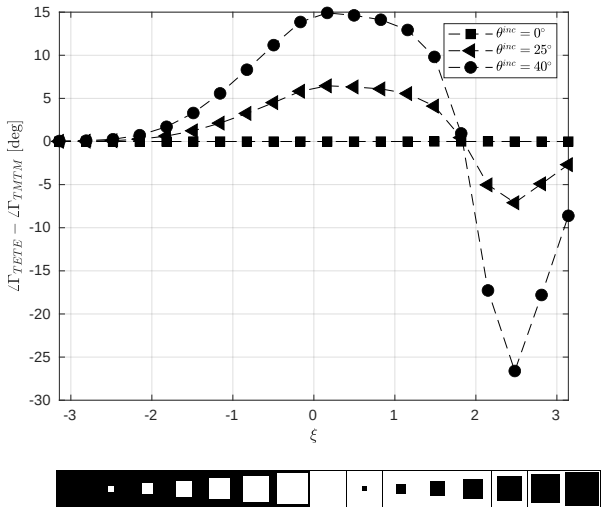

(b) Lookup table 1 cells depolarizing behavior with respect to different local incidence angles θ^{inc} at fixed $\phi^{inc} = -180°$.

Fig. 4: Lookup table 1 behaviour as function of the periodic parameter ξ describing the geometry. In the inset of (A) the relevant parameters defining the cell geometry.

and E_y^{refl} is matched one-by-one with a cell included in the lookup table able to reproduce a local reflected field with a minimum quadratic phase error compared to the ideal one.

The second step aims to minimize the amplitude error on the scattered far-field components through a multi-objective optimization of the RA layout [29], [30], [31]. It is done by describing the RA preliminary geometry distribution (obtained with the PO synthesis) with an unwrapped $2D$ ξ distribution. The ξ distribution on the RA surface is described through continuous tensorial spline representation [31], [32], and the optimization variables are therefore the bi-cubic splines coefficients, with the following advantages:

1) **Continuous modulation of cells geometries**: this description naturally avoids sharp geometric transitions on the RA surface. The quasi-periodicity constraint is, therefore, naturally respected.
2) **Reduction of the optimization problem d.o.f.**: the RA layout is described on a very limited set of knots compared to the actual number of cells composing the layout. The number of knots is directly related to the dimensions of the B-spline coefficients tensor whose elements are the optimization variables.

In the lookup tables, a local cubic interpolation of the scattering properties against the index of the cells (see section III-B) is performed to have fast access to the reflection matrices during the optimization process. The RA far-field components radiation pattern is computed through an in-house modified physical optics software [33]. The modified physical optics computation is performed by considering the local periodicity hypothesis, namely by characterizing the reflection matrix of each cell composing the database through the spectral domain MoM. This analysis technique has been successfully validated in several previous works from authors with respect to full-wave simulations [31] and measurements [17], [25], [34].

A general flowchart for the RF-mechanical coupled design is shown in Figure 5. This flowchart aims to give an overview of the RF-structural co-design and optimization illustrated in previous sections.

The RA1 (layout in Figures 6) radiation pattern in terms of LHCP component projected on Earth as seen from the satellite position are shown in Figure 7 and compared to the radiation pattern of a theoretic reference metallic shaped reflector. The results for the RHCP component are very similar and we omit the contour plot for brevity. Table IV summarizes the performances on stations comprised in the CONUS coverage region. $G_{CO_{max}}$ and $G_{X_{max}}$, are respectively the maximum co-polarization and cross-polarization gain on the stations, $G_{CO_{min}}$ is the minimum gain in the coverage region, XPD_{min} is the minimum cross-polarization discrimination on the stations, while $\overline{XPD}$ is the average cross-polarization discrimination evaluated on the ensemble of the stations. The performances of the RA1 are comparable with the reference reflector ones.

D. Impact of TED on the radiation pattern

Figure 8 shows the TED out-of-plane displacements of the complete RA in the deployed configuration, withstanding the transversal thermal gradient. The analysis is performed through the commercial finite elements method [19].

The impact on the radiation pattern is shown in Figure 9. The eclipse entering and eclipse exit load cases are almost equivalent in terms of the displacements' magnitude and the global impact on RF performances. The eclipse entering cold case is more critical compared to the other cases with out-of-plane displacement $RMS = 3.91$ mm. Nevertheless, the orders of magnitude are comparable among the four thermal load cases surveyed. The results obtained through the TED analysis of the RA FEM model point out that, at the present

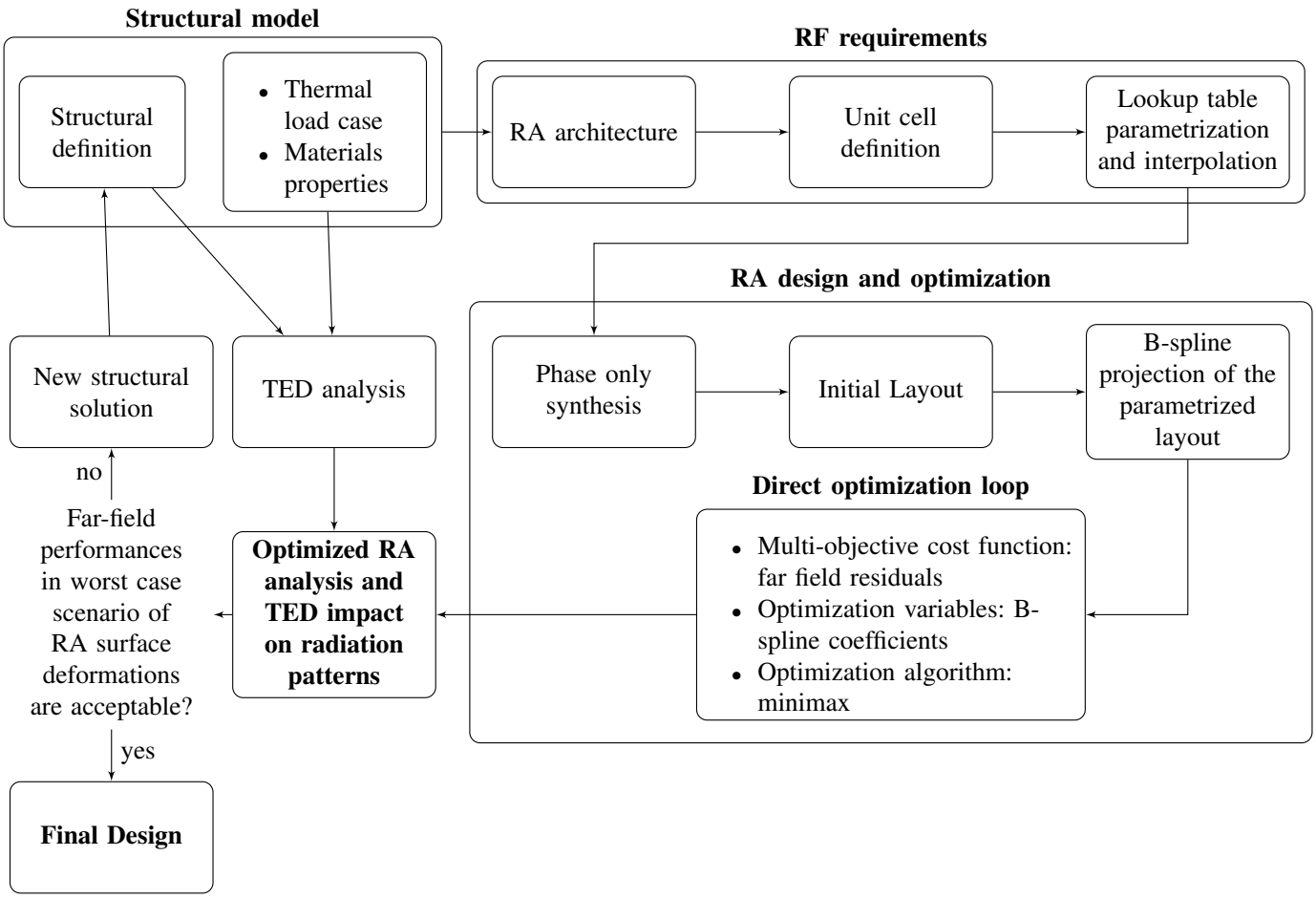

Fig. 5: Flow chart defining the RF/structural analysis and design process.

state, the RA shows about 3 dB losses in the coverage region in the worst-case TED configuration. The present analysis makes clear the necessity of a reorientation of the RA structural design, which in turns implies a reorientation of the RF design. To this extent, a structural and RF co-design is proposed in the next sections.

IV. RA ARCHITECTURE REORIENTATION

This section proposes a new solution to solve the TED issue by making the deployable panels more stable with respect to the transverse thermal gradient load case. The idea is based on the use of highly reliable and stable structures, such as carbon fiber reinforced polymers (CFRP) based sandwich panels, to support the RA reflecting panels (Figure 10a). The novel design implies, therefore, a separation of the mechanical and RF functions. To this extent, the backing structure ensures the thermo-mechanical stability of the RA, while the RA electric panel ensures the beam shaping. At a system level, this solution should respect one fundamental requirement, i.e., the equivalence in terms of the panels volume size in the folded configuration compared to the previous configuration (RA1). To this extent, the introduction of mechanical support has the remarkable consequence of considering the RA electric panels thinner than before.

From a structural dynamics requirement study performed through commercial software [19], the mechanical backing structure support should be 20 mm thick in order to be stiff enough and not interfere with the launcher/payload dynamics (antenna first structural eigenfrequency above 28 GHz). The mechanical support drives the overall panel stiffness, as can be expected. The electrical sandwich should be therefore reduced to 10 mm, in order to keep the same volumetric size of the RA in the folded configuration.

Figure 10a shows the new laminate layers structures. The same plies as in Figure 3 compose the RF sandwich, but with a reduced honeycomb spacer thickness (reduced here from $\lambda_0/4 = 30$ mm to $\lambda_0/12 = 10$ mm) and with only one ply of Astroquartz fabric, since the panel stiffening is provided by the mechanical support. The backing structure (that we also call "mechanical stage" from now on) is composed of a conventional sandwich panel characterized by two CFRP fabric skins on each side of an aluminum honeycomb. The advantage of the carbon fiber-based composite is that they are extremely stable with the temperature since their CTE is very low (average CFRP CTE $\approx 0.5 \times 10^{-6\circ} C^{-1}$, while for Astroquartz fabrics CTE $\approx 13 \times 10^{-6\circ} C^{-1}$).

An important aspect is how to connect the RF stage to the mechanical stage. Indeed, the direct bonding of the RF stage on the mechanical stage would not be acceptable since it would

This article has been accepted for publication in IEEE Transactions on Antennas and Propagation. This is the author's version which has not been fully edited and content may change prior to final publication. Citation information: DOI 10.1109/TAP.2023.3247940

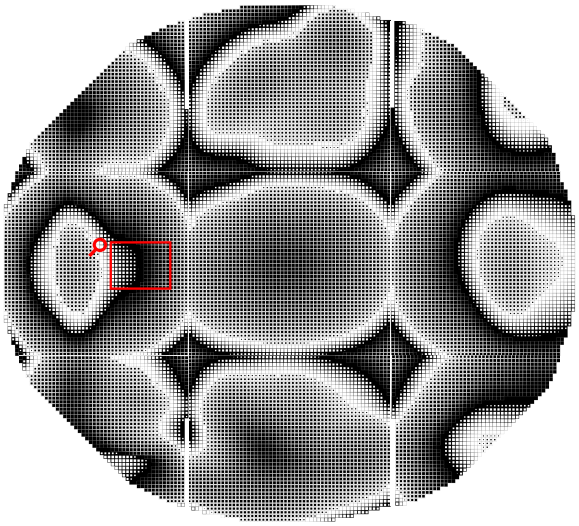

(a) RA1 layout composed of first and second order inductive Phoenix cells.

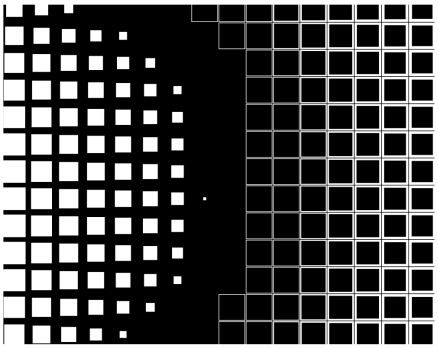

(b) Zoom.

Fig. 6: RA1 layout.

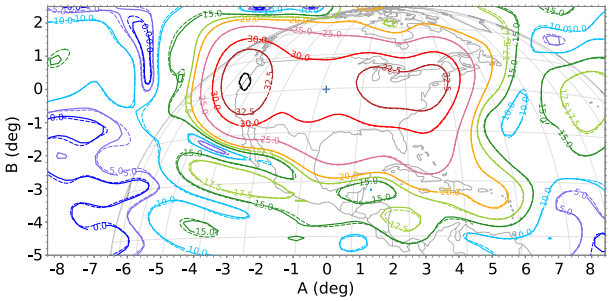

(a) Co-polarization component contour plot. Solid lines represent the RA1 far-field, dashed lines reference reflector far field.

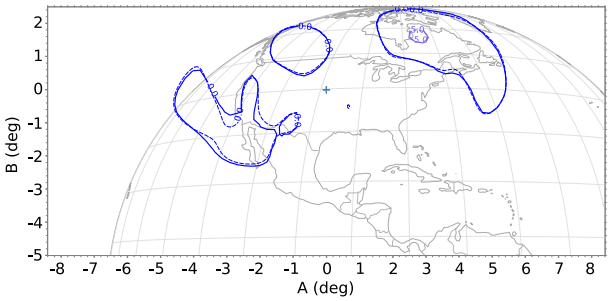

(b) Cross-polarization component contour plot. Solid lines represent the RA1 far-field, dashed lines reference reflector far field.

Fig. 7: RA1 performances.

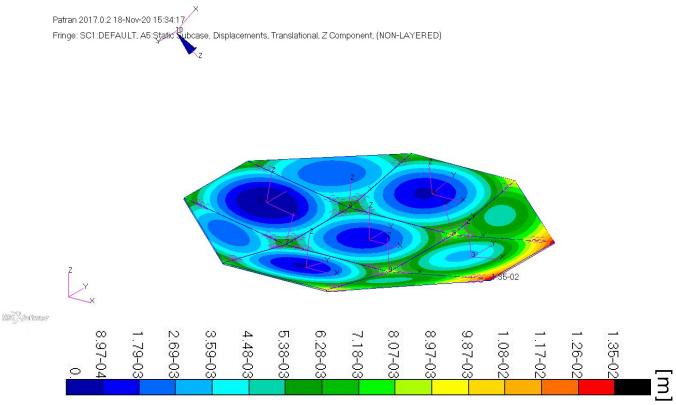

Fig. 8: TED on the deployed RA with self-standing structures under transversal gradient issued from the eclipse entering.

make the composites highly non-symmetric and would cause a bi-material effect that would result in a TED deformation even at room temperature [14], [21]. In this work, a solution based on the fragmentation of the RF stage in smaller panels the fixing to the mechanical stage through a system of bolts and in-plane sliding fixation is proposed (Figure 10b). The fragmentation is made to reduce the RF panels size to reduce the panels TED sensitivity. The fragmentation is conceived by letting a small gap of 5 mm between the adjacent panel to allow in-plane deformations. The sliding bolts are a heritage employed and demonstrated on a faceted Ku-band RA [17]. The sliding bolts allow the decoupling of the panels' in-plane deformations to the out-of-plane deformations, avoiding also the bi-material effect. Moreover, they allow the RA in-plane deformation, resulting in inhibited out-of-plane deformations, which, as indicated in the previous section III-D, is very degrading for the RA RF performances.

A. *FEM of the RA architecture reorientation*

The deployed RA is composed of nine CFRP skins/aluminum core honeycomb sandwich panels on which a total of thirty-two RF tiles are fixed. The hinges connect the backing structures, which become the support of the RA reflecting panels. The hinges and locking devices modeling is the same as reported in the previous section II-C. Once again, each panel is defined and analyzed in its local reference frame. Also, the boundary conditions are the same as presented in section II-C. The fixations and the sliding bolts connecting the mechanical stage and the RF stage are modeled through elastic interfaces (CELAS1 in Nastran). A highlight on the FEM interfaces for the rectangular and the corner panels is depicted in Figure 11.

B. *The thermal load*

The thermal load cases presented in section II-D are adapted to this new architecture by considering the worst-case and

This article has been accepted for publication in IEEE Transactions on Antennas and Propagation. This is the author's version which has not been fully edited and content may change prior to final publication. Citation information: DOI 10.1109/TAP.2023.3247940

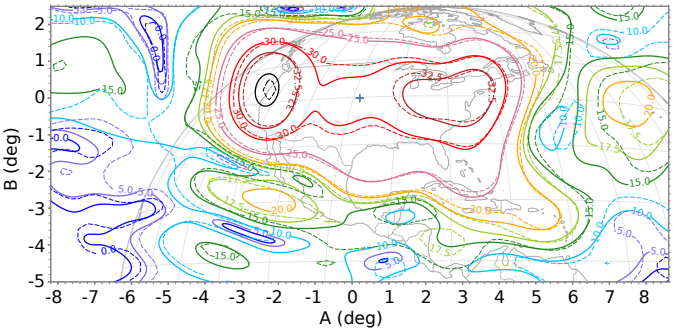

Fig. 9: Impact of the TED on the radiation pattern on the co-polarization component. RA1 in the deformed configuration solid line, RA1 in nominal configuration dashed lines.

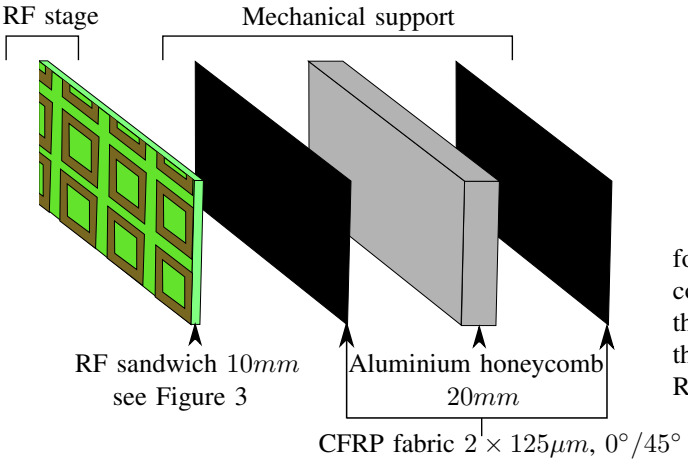

(a) RF stage and mechanical support composite panels layup.

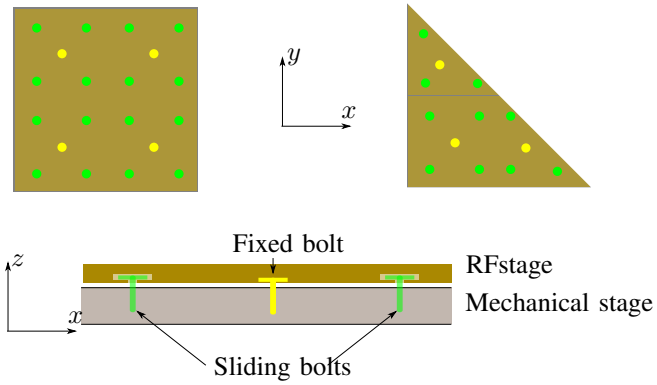

(b) Mechanical design proposition of the reoriented architecture. Upper view of the rectangular panel on the top left, and of the triangular corner panel on the top right. Side view on the bottom.

Fig. 10: Mechanical design reorientation of the deployable RA panels.

neglecting the composite materials' conductivity properties. The new load cases are an equal distribution of the total thermal gradient of $\Delta T = 20°\text{C}$ on the two stages.

C. TED analysis of the reoriented RA architecture

Figure 12 shows the complete RA model's TED with backing structures. The worst-case RMS out-of-plane displacements are reduced to 0.7 mm. The proposed solution allows

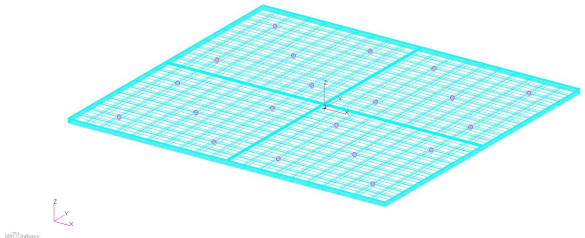

(a) Rectangular panel FEM.

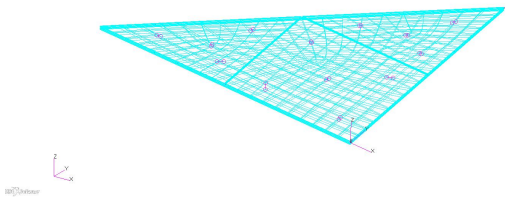

(b) Triangular corner panel FEM.

Fig. 11: FEM with the bolts interfaces highlight.

for thermoelastically stabilize the RA panels in the deployed configuration. The TED analysis shows a radical reduction of the out-of-plane maximum displacements. The TED impact on the RF performances is evaluated after presenting the new RA RF design in the next section.

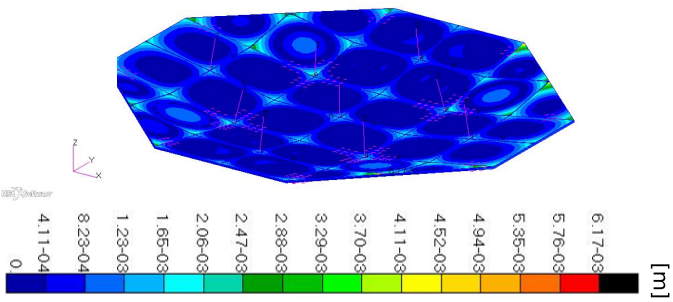

Fig. 12: TED on the deployed RA with a mechanical support under transversal gradient issued from the eclipse entering.

V. RA WITH A MECHANICAL SUPPORT DESIGN

A. New array constitutive elements and lookup table handling

By characterizing the cells of Figure 4, computed this time with a substrate thickness of $\lambda/12 = 10$ mm, we can notice a drastic change in the responses of the cells (Figure 13). The set of cells becomes more dispersive (a slight variation of the geometry implies a substantial reflection phase variation) and unstable in the region $\xi \in [2; \pi]$. Therefore, it is necessary to consider new cell geometries to grant the 360° reflection coefficient phase range while keeping the cells stability.

This article has been accepted for publication in IEEE Transactions on Antennas and Propagation. This is the author's version which has not been fully edited and content may change prior to final publication. Citation information: DOI 10.1109/TAP.2023.3247940

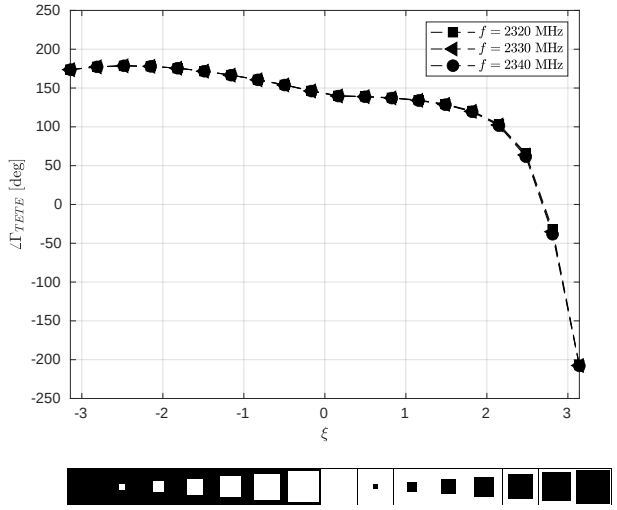

Fig. 13: The reflection phase of the cells geometries composing the lookup table 1 with a reduced substrate thickness ($\lambda_0/12$) as a function of the periodic parameter ξ describing the geometry.

The new Phoenix cycle adopted is composed of 2^{nd} and 4^{th} order inductive Phoenix cells. It is selected in order to avoid sharp geometrical transitions and to guarantee a full phase shift coverage. Figure 14a shows the behavior of the cells as a function of a new auxiliary periodic variable ξ defined as a linear parametrization of the four geometrical parameters of the Phoenix cells, $\mathbf{d} = \begin{bmatrix} d_1 & d_2 & d_3 & d_4 \end{bmatrix}$, as shown in the inset of Figure 14a. This allows the reduction of the cells degrees of freedom to just one. The lattice of the unit cell is $\lambda_0/3$, which corresponds to 43 mm.

In Figure 14a, the reflection phase is calculated under oblique plane wave incidence $\theta^{inc} = 25°$, $\phi^{inc} = -180°$ and displayed as a function of the parameter ξ. The phase variation shows that an almost complete $360°$ phase cycle is achieved, and the cells are clearly more stable with respect to the geometry variations (i.e. the parameter ξ). Since the cells are more influenced by the substrate impedance by considering a thinner substrate, it is worth evaluating the cells behavior under oblique incidence. To do so, we evaluate the cells principal reflection coefficient phase difference $\angle\Gamma_{TETE} - \angle\Gamma_{TMTM}$ for different θ^{inc} and $\phi^{inc} = -180°$. The resulting plot is shown in Figure 14b where we can notice that cells have a strong depolarizing effect at increasing incidence angles that affects the polarization purity of the far-field as shown in the next section. The increased depolarizing effect that the new lookup table cells globally experience is due essentially to the reduction of the substrate thickness imposed by mechanical design constraints. Analytical derivations of this phenomenon are available in [35], [36]. Indeed, the depolarization of the reflection on a bare grounded dielectric slab increases with a substrate thickness reduction. Therefore, independently from the considered PC geometry, the substrate impedance globally affects the depolarization of the reflected field components.

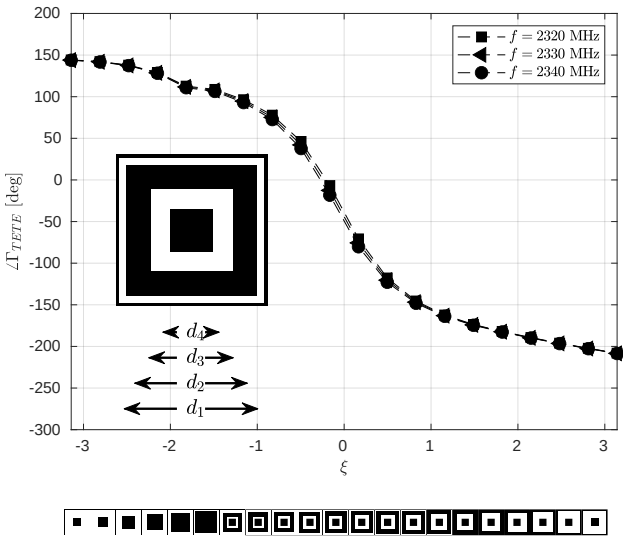

(a) Lookup table 2 cells reflection phase with respect to different frequencies at incidence $\theta^{inc} = 25°$ and $\phi^{inc} = -180°$.

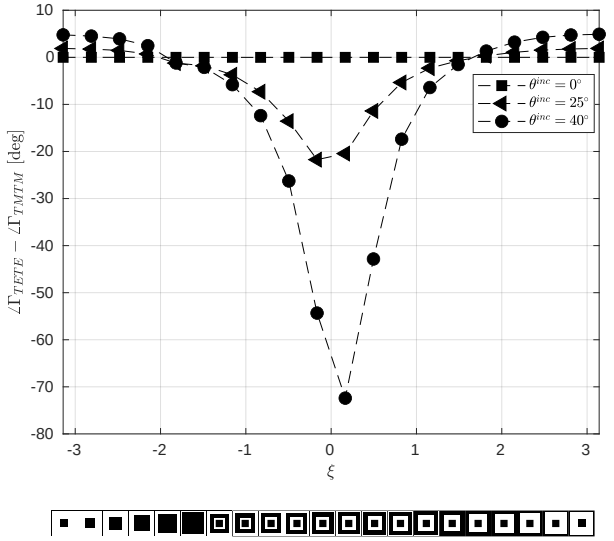

(b) Lookup table 2 cells depolarizing behavior with respect to different local incidence angles θ^{inc} at fixed $\phi^{inc} = -180°$.

Fig. 14: Lookup table 2 behaviour as function of the periodic parameter ξ describing the geometry. In the inset of (A) the relevant parameters defining the cell geometry.

B. New RA electrical design

The reduced thickness RA composed of the cells presented in the previous section is called RA2. Its performances are reported in table IV in comparison with the reference reflector performances. The cross-polarization levels of the RA2 design are very high and make the RA2 not competitive with respect to the reference reflector.

C. Improved cross-polarization new RA electrical design

By considering rectangular elements, it is possible to compensate for slight depolarizing effects [37].

To reduce the cross-polarization levels, the objective is now to minimize the maximum error between the radiation pattern and the prescribed mask by distorting the square cells geometry into rectangles ($d_x \neq d_y$). The RA layout is described through a continuous and derivable spline projection of the parameter ξ, identifying the cell index in the lookup table, and a cell distortion parameter h. The optimization variables are therefore the spline coefficients of the two surfaces describing the parametrized cells distribution [32]. A *minimax* algorithm allows minimizing the maximum of the vectorial cost function described as the error on the radiation pattern amplitude with respect to the mask and the maximization of the XPD levels. The initial condition is the single polarization design of section V-B.

TABLE IV: Performances comparison.

	Reference reflector	RA1	RA2	RA3
$G_{CO_{max}}$	35.14 dB	34.98 dB	34.75 dB	34.66 dB
$G_{CO_{min}}$	25.44 dB	25.71 dB	25.25 dB	24.52 dB
$G_{X_{max}}$	5.28 dB	5.69 dB	18.07 dB	6.09 dB
XPD_{min}	24.18 dB	21.15 dB	9.46 dB	21.98 dB
$\overline{XPD}$	34.54 dB	33.39 dB	19.74 dB	34.16 dB

The radiation pattern in terms of 2D contour plots projected on Earth as seen from the satellite position associated with the new RA3 layout of Figure 15a is shown in Figure 16 in comparison with those obtained with the reference reflector. The cross-polarization levels have maximum values comparable to the reference reflector. Moreover, from Table IV the average XPD distribution on the stations has been improved by 14 dB with respect to the RA2 layout composed of square cells. We can notice that the reduction of the cross-polarization levels is accompanied by a slight degradation of the co-polarization component. Table IV presents the RA3 performances. The maximum levels of the co-polarized, and cross-polarization components gain are comparable with those obtained with the reference reflector.

The impact of the TED previously presented in section IV is now evaluated. From Figure 17 we can see that the radiation pattern is not affected by the surface displacements issued from the thermo-elastic deformations of section IV, demonstrating the effectiveness of the concept. Moreover, the total surface mass of the RA with mechanical support is 3.02 Kg/m2, while the RA with self-standing structures shows a total surface mass of 2.99 Kg/m2. The mass budgets of the two structural configurations are therefore comparable, such as their volumetric sizes in the stowed configuration.

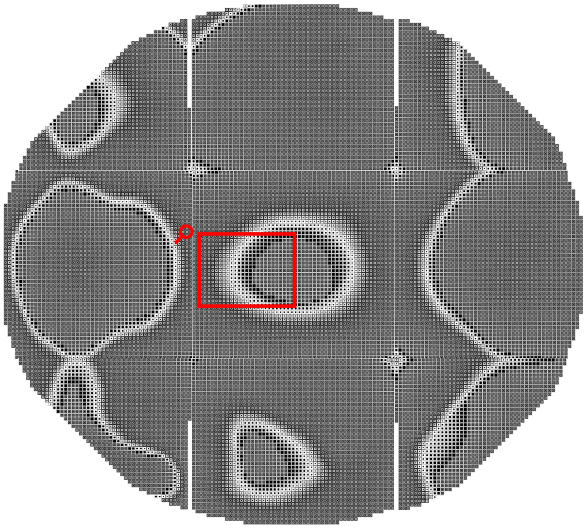

(a) RA3 layout composed of second and fourth order rectangular Phoenix cells.

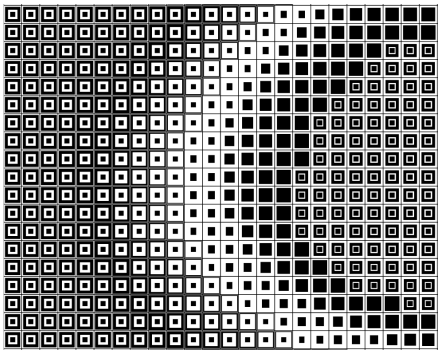

(b) Zoom.

Fig. 15: RA3 layout.

VI. Conclusions

This paper proposes a novel RF-mechanical coupled design approach in order to mitigate the in-orbit thermo-elastic distortions of large deployable RA. This concept is based on introducing a mechanical support conceived with simple and reliable structures, less sensitive to TED. This mechanical design reorientation has shown a radical reduction of the TED, and therefore their impact on the RA performances. The main drawback of the proposed mechanical reorientation is the reformulation of the electrical architecture of the RA. Indeed a reduced thickness RF panel is needed in order to keep the same total thickness of the panels in the stowed configuration for the novel solution compared to the conventional one.

The three S-band deployable RAs designed in this paper have shown interesting features. The RA1 has been designed by considering a RA with a classical self-standing structure, with a substrate thickness of $\lambda_0/4 = 30$ mm. In this configuration, first and second-order inductive Phoenix cells have been employed, resulting in a RA layout presenting good features compared to the reference reflector. On the other hand, the RF design presents added complexity for the RA with the new mechanical support. Indeed the RA substrate reduction to $\lambda_0/12 = 10$ mm implies a dispersive behavior of the first and second-order Phoenix cells. This issue is addressed by employing second and fourth-order inductive Phoenix cells. The resulting new lookup table cells have shown a depolarizing effect when withstanding an oblique incident field, resulting in high cross-polarization levels for

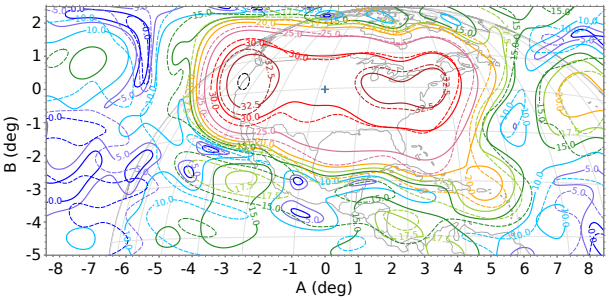

(a) Co-polarization component contour plot. Solid lines represent the RA3 far-field, dashed lines reference reflector far field.

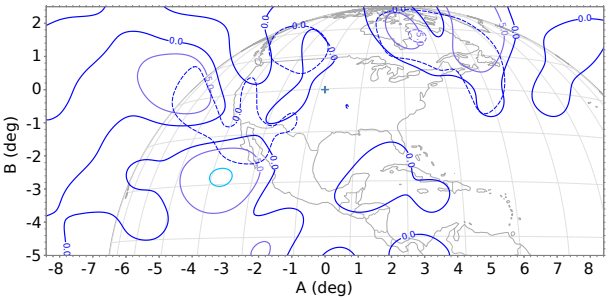

(b) Cross-polarization component contour plot. Solid lines represent the RA3 far-field, dashed lines reference reflector far field.

Fig. 16: RA3 performances.

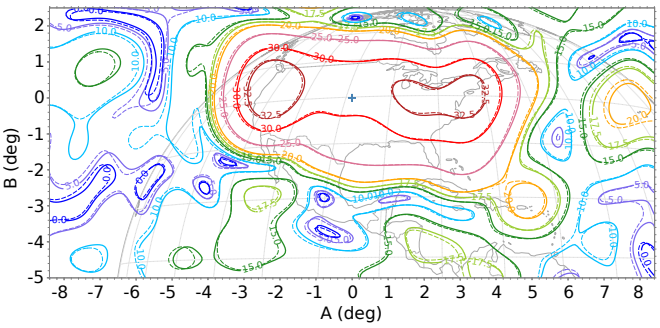

Fig. 17: Impact of the TED on the radiated co-polarization component. RA3 in the deformed configuration solid line, RA3 in nominal configuration dashed lines.

RA2 design. An enhancement of the cells lookup table is then proposed to mitigate the cross-polarization increase. A supplementary degree of freedom is added in the elementary cell design by considering square Phoenix cells deformed into rectangles. The RA3 layout shows reduced cross-polarization levels compared to the previous low-profile RA design with mechanical support. The average XPD is enhanced by 14 dB compared to the layout composed of square cells. Moreover, the new RA architecture is very stable to TED phenomena demonstrating the effectiveness of the proposed coupled RF/mechanical design.

REFERENCES

[1] R. Chiniard, L. Schreider, N. Girault, S. Vezain, E. Labiole, G. Caille, Y. Baudasse, H. Legay, and D. Bresciani. Study of a very large reflectarray antenna built with unfoldable panels for missions from l to c band. *CEAS Space J.*, 5(3-4):233–242, 2013.

[2] M. Arya, J. F Sauder, R. Hodges, and S. Pellegrino. Large-area deployable reflectarray antenna for cubesats. In *AIAA Scitech 2019 Forum*, page 2257, 2019.

[3] M.W. Thomson. The astromesh deployable reflector. In *IEEE Antennas and Propag. Soc. Int. Symp.*, volume 3, pages 1516–1519 vol.3, 1999.

[4] G. L Davis and R. L. Tanimoto. Mechanical development of antenna systems. *Spaceborne Antennas for Planet. Exploration*, pages 425–454, 2006.

[5] Y. Zhang, B. Dong, G. Yang, D. Yang, and S. Zhang. Design technique for a shaped-reflector antenna with a three-layer cable net structure. *IEEE Trans. on Antennas and Propag.*, 69(1):109–121, 2021.

[6] J. Huang and J. A. Encinar. *Reflectarray antennas*. John Wiley & Sons, 2007.

[7] L. Datashvili, H. Baier, J. A. Encinar, and H. Legay. Mechanical investigation of a multi-layer reflectarray for ku-band space antennas. *Aerosp. Sci. and Technol.*, 10(7):618–627, 2006.

[8] J. A. Encinar, L. S. Datashvili, J. A. Zornoza, M. Arrebola, M. Sierra-Castaner, J. L. Besada-Sanmartin, H. Baier, and H. Legay. Dual-polarization dual-coverage reflectarray for space applications. *IEEE Trans. on Antennas and Propag.*, 54(10):2827–2837, 2006.

[9] J. A. Encinar, M. Arrebola, L. F. de la Fuente, and G. Toso. A transmit-receive reflectarray antenna for direct broadcast satellite applications. *IEEE Trans. on Antennas and Propag.*, 59(9):3255–3264, 2011.

[10] N. Chahat, E. Thiel, J. Sauder, M. Arya, and T. Cwik. Deployable one-meter reflectarray for 6u-class cubesats. In *2019 13th Eur. Conf. on Antennas and Propag. (EuCAP)*, pages 1–4, 2019.

[11] R. E. Hodges, D. J. Hoppe, M. J. Radway, and N. E. Chahat. Novel deployable reflectarray antennas for cubesat communications. In *2015 IEEE MTT-S Int. Microw. Symp.*, pages 1–4, 2015.

[12] R. E. Hodges, N. Chahat, D. J. Hoppe, and J. D. Vacchione. A deployable high-gain antenna bound for mars: Developing a new folded-panel reflectarray for the first cubesat mission to mars. *IEEE Antennas and Propag. Mag.*, 59(2):39–49, 2017.

[13] R. E. Hodges, J. C. Chen, M. R. Radway, L. R. Amaro, B. Khayatian, and J. Munger. An extremely large ka-band reflectarray antenna for interferometric synthetic aperture radar: Enabling next-generation satellite remote sensing. *IEEE Antennas and Propag. Mag.*, 62(6):23–33, 2020.

[14] S. Timoshenko. Analysis of bi-metal thermostats. *Josa*, 11(3):233–255, 1925.

[15] C. Collier. Stiffness, thermal expansion, and thermal bending formulation of stiffened, fiber-reinforced composite panels. In *34th Struct., Struct. Dyn. and Mater. Conf.*, page 1569, 1993.

[16] M. Arya, R. Hodges, J. F Sauder, S. Horst, M. Mobrem, A. Pedivellano, A. Wen, A. Truong, and S. Pellegrino. Lightweight composite reflectarray that can be flattened, folded, and coiled for compact stowage. In *AIAA SCITECH 2022 Forum*, page 1886, 2022.

[17] H. Legay, D. Bresciani, E. Labiole, R. Chiniard, and R. Gillard. A multi facets composite panel reflectarray antenna for a space contoured beam antenna in ku band. *Prog. In Electromagn. Res.*, 54:1–26, 2013.

[18] S. Vezain, Y. Baudasse, N. Dando, and L. Schreider. Large rigid deployable structures and method of deploying and locking such structures, October 8 2013. US Patent 8,550,407.

[19] MSC Nastran. User's guide. *MSC Software corporation*, 2012.

[20] H. Legay, D. Bresciani, E. Girard, R. Chiniard, E. Labiole, O. Vendier, and G. Caille. Recent developments on reflectarray antennas at thales alenia space. In *2009 3rd Eur. Conf. on Antennas and Propag.*, pages 2515–2519, 2009.

[21] Stephen W Tsai. *Theory of composites design*. Think composites Dayton, 1992.

[22] JPS Composite Materials. *Technical Reference Handbook*, 2017.

[23] L. Moustafa, R. Gillard, F. Peris, R. Loison, H. Legay, and E. Girard. The phoenix cell: A new reflectarray cell with large bandwidth and rebirth capabilities. *IEEE Antennas and Wireless Propag. Lett.*, 10:71–74, 2011.

[24] A. Guarriello, G. Courtin, R. Loison, and R. Gillard. A general equivalent circuit model for phoenix cells. *IEEE Trans. on Antennas and Propag.*, 69(11):7982–7986, 2021.

[25] L. Marnat, R. Loison, R. Gillard, D. Bresciani, and H. Legay. Comparison of synthesis strategies for a dual-polarized reflectarray. *Int. J. of Antennas and Propag.*, 2012, 2012.

[26] D. Bresciani. A unified approach to the characterization of frequency and polarization selective surfaces. In *Proc. of IEEE Antennas and Propag. Soc. Int. Symp.*, pages 1960–1963 vol.3, 1993.

[27] S. Contu and R. Tascone. Scattering from passive arrays in plane stratified regions. *Electromagn.*, 5(4):285–306, 1985.

[28] Jianxun Su, Yao Lu, Hui Zhang, Zengrui Li, Yongxing Che, Kainan Qi, et al. Ultra-wideband, wide angle and polarization-insensitive specular reflection reduction by metasurface based on parameter-adjustable meta-atoms. *Scientific rep.*, 7(1):1–11, 2017.

[29] M. Zhou, S. B. Sørensen, O. S. Kim, E. Jørgensen, P. Meincke, and O. Breinbjerg. Direct optimization of printed reflectarrays for contoured beam satellite antenna applications. *IEEE Trans. on Antennas and Propag.*, 61(4):1995–2004, 2013.

[30] M. Zhou, S. B. Sørensen, O. S. Kim, E. Jørgensen, P. Meincke, O. Breinbjerg, and G. Toso. The generalized direct optimization technique for printed reflectarrays. *IEEE Trans. on Antennas and Propag.*, 62(4):1690–1700, 2014.

[31] V. Richard, R. Loison, R. Gillard, H. Legay, M. Romier, J.-P. Martinaud, D. Bresciani, and F. Delepaux. Spherical mapping of the second-order phoenix cell for unbounded direct reflectarray copolar optimization. *Prog. In Electromagn. Res. C*, 90:109–124, 2019.

[32] A. Guarriello, D. Bresciani, H. Legay, G. Goussetis, and R. Loison. Design of circularly polarized and highly depointing reflectarrays with high polarization purity. In *2022 16th Eur. Conf. on Antennas and Propag. (EuCAP)*, pages 1–5, 2022.

[33] D. Bresciani and S. Contu. Scattering analysis of dichroic subreflectors. *Electromagn.*, 5(4):375–407, 1985.

[34] S. Mercader-Pellicer, G. Goussetis, G. M. Medero, H. Legay, D. Bresciani, and N. J. G. Fonseca. Cross-polarization reduction of linear-to-circular polarizing reflective surfaces. *IEEE Antennas and Wireless Propagation Letters*, 18(7):1527–1531, 2019.

[35] C. A. Balanis. *Advanced engineering electromagnetics*. John Wiley & Sons, 2012.

[36] O. Luukkonen, C. R Simovski, and S. A. Tretyakov. Grounded uniaxial material slabs as magnetic conductors. *Prog. In Electromagn. Res. B*, 15:267–283, 2009.

[37] D. Bresciani, H. Legay, E. Labiole, and G. Caille. Antenne réseau réflecteur à compensation de polarisation croisée et procédé de réalisation d'une telle antenne. *Patent FR*, 1001100, 2011.

Andrea Guarriello received the M.Sc. double degree (cum laude) in Space and Astronautical engineering from Sapienza University, Rome, Italy, and the Institut Supérieur de l'Aéronautique et de l'Espace (ISAE-Supaero), Toulouse, France, in 2016, the Research Master degree in Aerospace Structures and Materials from ISAE-Supaero, Toulouse, France, in 2016. He received the Ph.D. degree in electrical engineering from National Institute of Applied Science (INSA), Rennes, France, and Heriot-Watt University, Edinburgh, U.K., in 2021.

His Ph.D. research was part of the doctorate program REVOLVE under the European Commission's H2020 Marie Skłodowska-Curie Actions and carried out in part at the Research and Technologies Department, Thales Alenia Space, Toulouse, France. Since fall 2021 he is a research engineer at Institut d'Électronique et des Technologies du numéRique (IETR) in Rennes, France. His current research interests include the developments of models and computer codes for reflectarrays analysis and optimization, the analysis and design of periodic and quasi-periodic metasurfaces, the mechanical and electrical codesign of large reflectarray antennas for space applications with emphasis on deployable structures.

Renaud Loison is professor at the Institut National des Sciences Appliquées (INSA), Rennes, France. He carries out his research activity at the Institut d'Électronique et des Technologies du numéRique (IETR) and works on reflectarrays, metasurfaces and more generally on periodic and quasi-periodic surfaces.

Daniele Bresciani was born on February the 27th, 1958. He graduated in 1982 at Politecnico di Torino, Italy.

His fields of Interest are study, analysis and design of reflector antenna systems with particular emphasis on Reflectarrays and Frequency or Polarization Selective Surfaces (FSS or Dichroics), for applications such as satellite communications (radio links, terrestrial coverages, etc); development of theoretical models and computer codes aimed to electromagnetic design and graphic applications.

His major skills are reflectarrays and FSS study and design, complex reflector systems analysis, dielectric and dichroic lenses synthesis and analysis, near field fast reconstruction. His present job is at Thales Alenia Space France in Toulouse at Research Department, carrying on studies and codes development on reflect-array subject (electrical design and measurements).

Hervé Legay received the Electrical Engineering and Ph.D. degrees from the National Institute of Applied Sciences, Rennes, France, in 1988 and 1991, respectively.

He was then a Post-Doctoral Fellow with the University of Manitoba, Winnipeg, MB, Canada. In 1994, he joined Alcatel Space (now Thales Alenia Space), Toulouse, France. He initially conducted studies in the areas of military telecommunication satellite antennas and antenna processing. He designed the architecture and the antijamming process of the first space active antenna (Syracuse 3 Program). He is currently the head of Research on space antennas, developing disruptive antenna concepts with emerging technologies, and associated systems in telecommunication and navigation. He conducted major developments on reflectarrays, full metal RF metasurfaces, integrated and low profile antennas, multiple beam quasi-optical beamformers. His center of interest includes also innovative active antenna architectures and system activities related to the monitoring of active antennas.

He is a Co-Director of the joint laboratory MERLIN, involving Thales Alenia Space, and the Institut d'Electronique et de Télécommunication de Rennes, which is located in Toulouse and Rennes. He is the Chair of the group of antenna experts at Thales Group. He coordinates collaborations with academic and research partners. He has authored 46 patents. Dr. Legay was a co-prize winner of the 2007 Schelkunoff Prize Paper Award. He was a recipient of the Gold Thales Awards in 2008, a reward for the best innovations in the Thales Group.

George Goussetis (S 99, M 02, SM 12) received the Diploma degree in Electrical and Computer Engineering from the National Technical University of Athens, Greece, in 1998, and the Ph.D. degree from the University of Westminster, London, UK, in 2002. In 2002 he also graduated B.Sc. in physics (first class) from University College London (UCL), UK. In 1998, he joined the Space Engineering, Rome, Italy, as RF Engineer and in 1999 the Wireless Communications Research Group, University of Westminster, UK, as a Research Assistant. Between 2002 and 2006 he was a Senior Research Fellow at Loughborough University, UK. He was Assistant Professor with Heriot-Watt University, Edinburgh, UK between 2006 and 2009 and Associate Professor with Queen's University Belfast, UK, between 2009 and 2013. In 2013 he joined Heriot-Watt and was promoted to Professor in 2014. He is currently the director of the Institute of Sensors Signals and Systems at Heriot-Watt University. He has authored or co-authored over 500 peer-reviewed papers several book chapters one book and six patents. His research interests are in the area of microwave and antenna components and subsystems with particular focus on their applications in satellite communication systems. Dr. Goussetis held research fellowships from the Onassis foundation in 2001, the UK Royal Academy of Engineering between 2006-2011, and European Commission Marie-Curie in 2011-12 and again in 2014-17. He is the recipient of several awards including the 2011 European Space Agency young engineer of the year prize and the 2016 Bell Labs prize. Dr. Goussetis served as Associate Editor to the IEEE Antennas and Wireless Propagation Letters between 2014-18 and is the Chair of EuCAP 2024.